<div align="center">

Electronic Supplementary Information

Cobalt-based metal organic framework：a highly active oxidase-mimicking nanozyme for fluorescence "turn-on" assay of biothiol

</div>

<div align="center">

Tian Jin, Yilei Li, Wenjie Jing, Yunchao Li, Louzhen Fan, Xiaohong Li*

Key Laboratory of Theoretical and Computational Photochemistry, Ministry of Education, College of Chemistry, Beijing Normal University, Beijing, 100875, China.

</div>

Tel: +86-10-58802741

E-mail: lxhxiao@bnu.edu.cn

Experiments

Chemicals

CH_3OH and CH_3CH_2OH were purchased from Beijing Chemical Works. CH_3COOH was purchased from Beijing Tongguang Fine Chemicals Company. Amplex red (AR) was purchased from Beijing Bai-Ao Lai-Bo Technology Co., Ltd. CH_3COONa, L-cysteine (L-Cys), phenylalanine (Phe), aspartic (Asp), glutamic (Glu), methionine (Met), lysine (Lys), glycine (Gly), $Co(NO_3)_2 \cdot 6H_2O$, 2-methylimidazole ($C_4H_6N_2$), 3, 3', 5, 5'-tetramethylbenzidine (TMB) and 2, 2'-azino-bis (3-ethylbenzthiazoline-6-sulfonic acid) (ABTS) were purchased from Aladdin Industrial Corporation (Shanghai, China). All chemicals were used as received without further purification. Deionized water was used in all experiments.

Preparation of ZIF-67

ZIF-67 was synthesized according to the literatures[S1]. 60 mg Co $(NO_3)_2 \cdot 6H_2O$ was dissolved in 30 mL CH_3OH to form a pink solution. 1 g 2-methylimidazole ($C_4H_6N_2$) was dissolved in 30 mL CH_3OH. To the pink solution, the $C_4H_6N_2$ solution was rapidly added with colour switching into purple quickly. Subsequently, the mixture was stirred for 30 s, and kept static for 24 h at room temperature. The final

mixture was centrifuged and washed with CH_3OH for five times.

Characterization

The morphology of as-prepared ZIF-67 was characterized with field-emission scanning electron microscope (FE-SEM) (Hitachi S4800 instrument equipped spectrometers), high-resolution electron microscopy (HRTEM) (JEOL JEM 2100 transmission electron microscope). The composition was analyzed by energy-dispersive X-ray spectroscopy (EDX) attached to FESEM instrument. X-ray diffraction (XRD) analysis was carried out by Rigaku D/max-2400 diffractometer operating at 40 kV and 200 mA current using CuKα radiation (l = 1.5418 Å). N_2 sorption isotherms and Brunauer–Emmett–Teller (BET) surface areas were measured at 77 K with an ASAP 2020 physisorption analyzer (USA). The fluorescence spectra was collected with a fluorescence spectrometer (Model FS5). The absorption spectroscopy was evaluated by using a UV-2450 spectrophotometer.

Oxidase-like property of ZIF-67 with TMB and ABTS as substrates

Typically, 50 μL TMB in DMSO solution (20 mM) and 50 μL as-prepared ZIF-67 suspension (20 mg□mL^{-1}) were successively injected into 900 μL buffer solution (20 mM NaAc-HAc, pH = 4.0) at room temperature. After 10 min, the oxidized product was evaluated by UV-Vis spectra with wavelength from 500 – 800 nm. At the same time, N_2 was used to partially remove resolved O_2 for 10 min, and further evaluated by UV-Vis spectra. Similarly, ABTS was used instead of TMB, and the oxidized product was evaluated by UV-Vis spectra with wavelength from 375 – 475 nm.

For steady-state kinetics, keeping C_{ZIF-67} at 1 mg□mL^{-1} and varying C_{TMB} (from 0.06 mM to 0.4 mM) with final volume of 1 mL, the initial oxidation reaction velocity of TMB was obtained by monitoring the absorbance at 653 nm for 1 min. The kinetic parameters, $[K_m]$ and $[V_{max}]$, were calculated by the Line weaver–Burk plot (derived from the Michaelis–Menten equation), shown as $1/\upsilon = K_m/V_{max}□(1/[S] + 1/K_m)$, where υ is initial reaction velocity, K_m is Michaelis constant, V_{max} is maximal initial reaction velocity, and [S] is substrate concentration.

For L-cysteine detection, 50 μL ZIF-67 suspension (20 mg□mL^{-1}) was mixed with 50 μL TMB in DMSO solution (20 mM) in a buffer solution (20 mM NaAc-HAc, pH = 4.0) for 10 min. Upon ZIF-67 being centrifuged and separated, L-cysteine (0-300 μM) was added to the supernatant. The mixtures were incubated for 10 min, and then recorded by UV-Vis spectra. As for selectivity towards L-cysteine, $C_{L-cysteine}$ was fixed at 100 μM, and the concentrations of other amino acids (phenylalanine, aspartic,

glutamic, methionine, lysine and glycine) were kept at 1 mM, respectively.

Oxidase-like property of ZIF-67 with AR as a substrate

10 μL AR in DMSO solution (100 μM) and 50 μL ZIF-67 suspension (20 mg□mL^{-1}) were successively injected into 940 μL of buffer solution (20 mM NaAc-HAc, pH = 4.0) at room temperature. The oxidized product of AR was recorded by fluorescence spectra at 5 min. At the same time, N$_2$ was used to partially remove resolved O$_2$ for 5 min, and further evaluated by fluorescence spectra.

For steady-state kinetics experiment, keeping C_{ZIF-67} at 1 mg□mL^{-1} and varying C_{AR} from 0.2 μM to 5 μM with a final volume of 1 mL, the initial oxidation reaction velocity of AR was obtained by monitoring the emission intensity at 585 nm for 1 min.

For L-cysteine detection, 50 μL ZIF-67 suspension (20 mg□mL^{-1}) was mixed with 10 μL AR in DMSO solution (100 μM) in a buffer solution (20 mM NaAc-HAc, pH = 4.0) for 100 min. Upon ZIF-67 being centrifuged and sepearted, varied $C_{L-cysteine}$ (0 - 300 μM) was added to the supernatant. The mixtures were incubated for another 80 min. The resultant solution was recorded by fluorescence spectra. As for the study of the selectivity toward L-cysteine, $C_{L-cysteine}$ was fixed at 100 μM, and concentrations of other amino acids (phenylalanine, aspartic, glutamic, methionine, lysine and glycine) were kept at 1 mM, respectively.
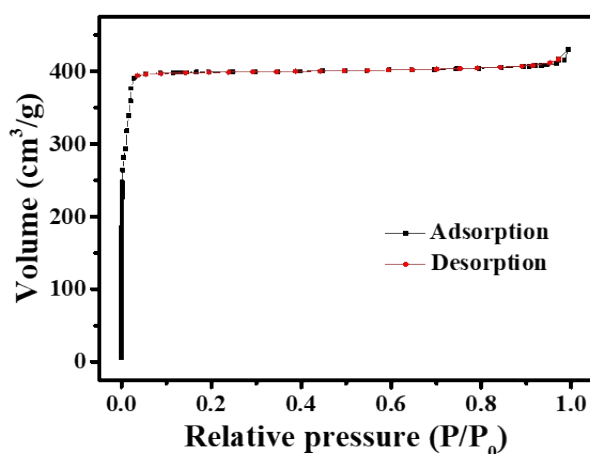

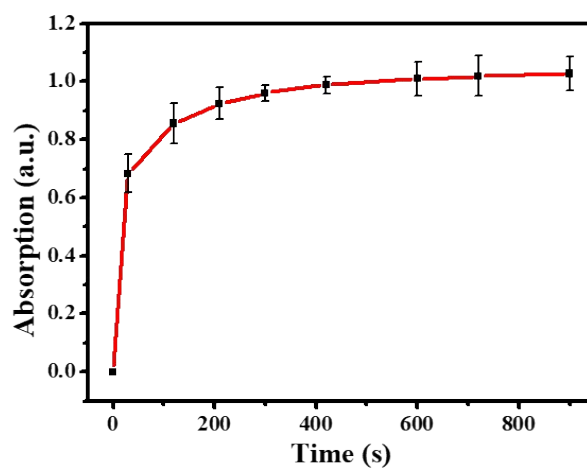**Fig S1.** N$_2$ adsorption-desorption isotherms of ZIF-67

Fig. S2. UV/Vis spectra of TMB-ZIF-67 system varies with time. Error bars represent the standard deviations from at least 3 measurements.
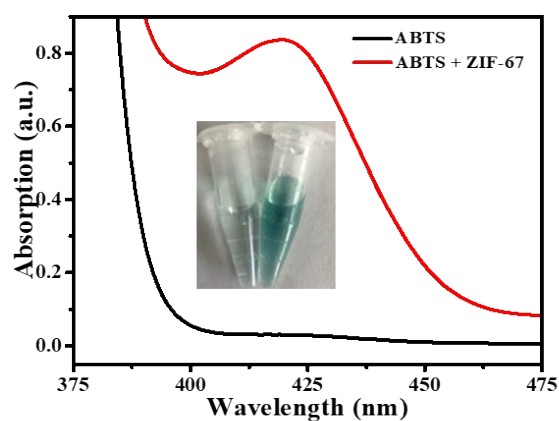

Fig S3. UV/Vis spectra and the corresponding optical photographs of ABTS in the absence and presence of 1 mg/mL ZIF-67 in a buffer solution (20 mM NaAc-HAc, pH = 4.0).
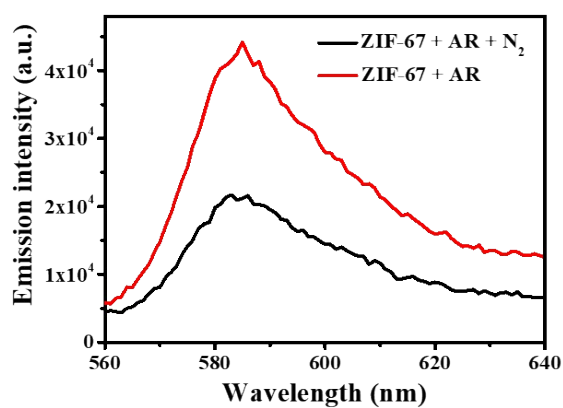

Fig. S4. Fluorescence spectra of AR-ZIF-67 system before (red line) and after (black line) exposed to N_2 in a buffer solution (20 mM NaAc-HAc, pH = 4.0).
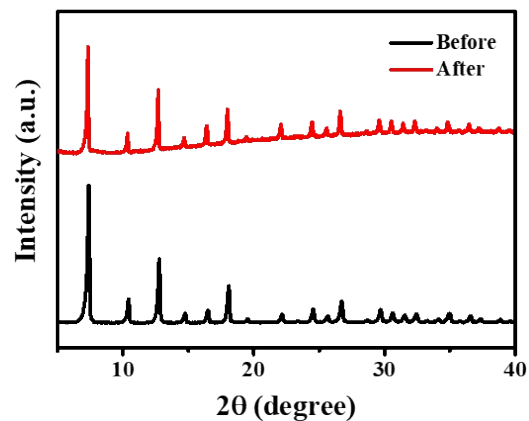
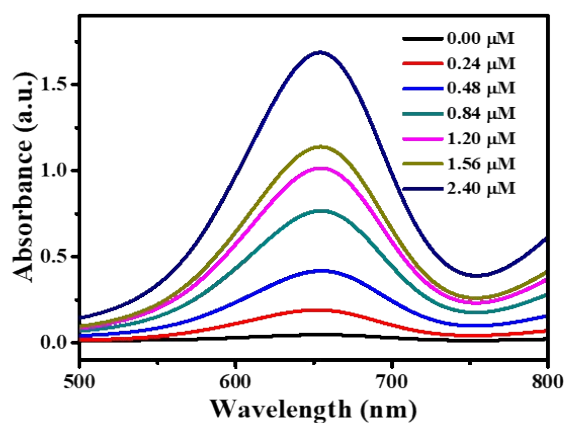Fig. S5. PXRD patterns of ZIF-67 before and after the catalytic oxidation of TMB by resolved O_2.

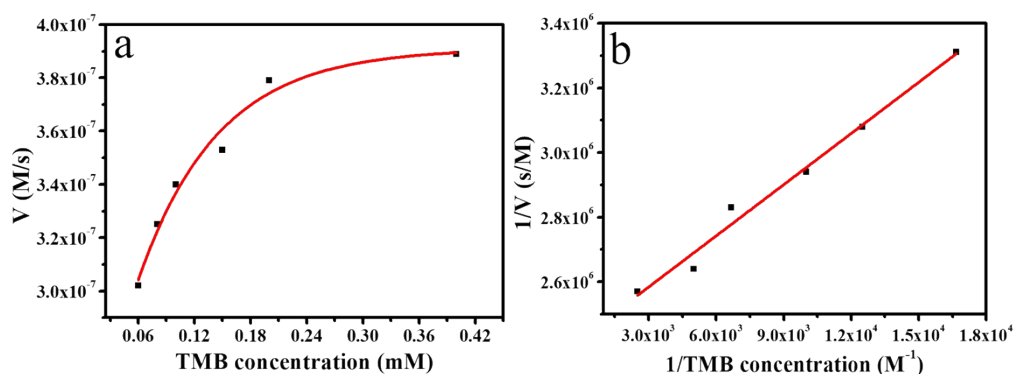**Fig. S6.** UV-Vis spectra of TMB-ZIF-67 system varies with C_{ZIF-67}.

Fig. S7. (a) Steady-state kinetic assays of ZIF-67, and (b) the corresponding double reciprocal plots. The concentration of TMB varies from 0.06 mM to 0.4 mM.

Table S1. Compared kinetic parameters with other oxidase mimics with TMB as a substrate

Oxidase mimics	K_m	Reference
Pt nanoclusters	0.630 mM	S2
MnO_2	0.04 mM	S3
CeO_2 nanoparticles	0.8 – 3.8 mM	S4
Ir/NC	0.0036 mM	S5
Ni–Pd hollow nanoparticles	0.11 mM	S6
Fe_3C/N-Doped Carbon Nanofibers	0.225 mM	S7
ZIF-67	**0.022 mM**	**This work**
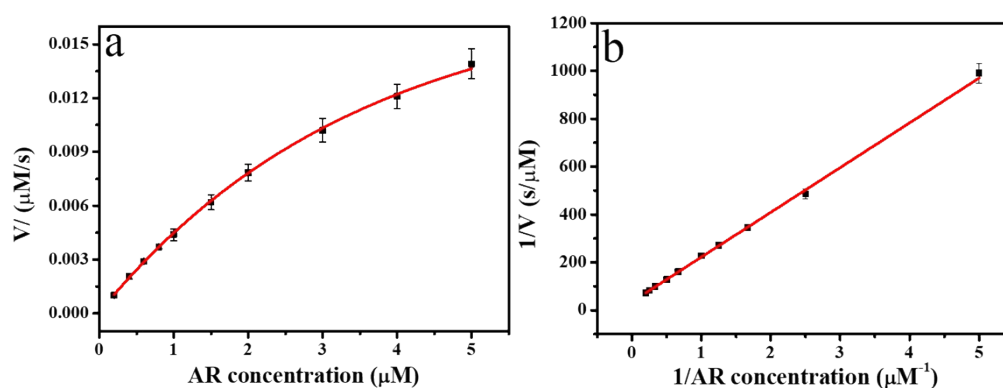
Fig. S8. (a) Steady-state kinetic assays of ZIF-67 (b) the corresponding double reciprocal plots. AR concentration varied from 0.2 μM to 5 μM. Error bars represent the standard deviations from at least 3 measurements.

Table S2. Compared kinetic parameters with natural enzymes and nanozymes with AR as a substrate

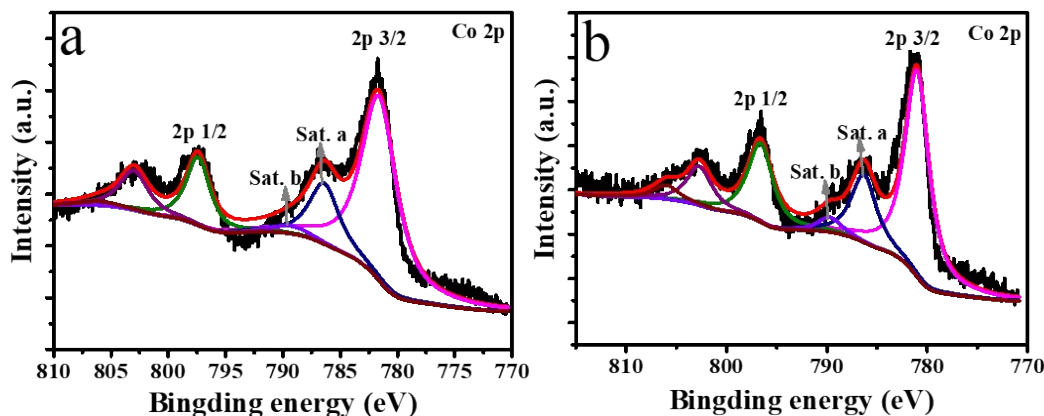| Catalyst	K_m	Reference
HRP	94.9 μM	S8
Bi–Au NPs	89.3 μM	S8
$Pt_{0.1}$/Au NPs	113 μM	S9
CoO_xH-GO	4.87 μM	S10
NiO	0.62 μM	S11
ZIF-67	**5.28 μM**	**This work**

Fig. S9. XPS spectra of ZIF-67 before (a) and after (b) the catalytic oxidation of TMB by resolved O_2.

The XPS before and after the reaction are shown as Fig S9. For the high-resolution spectrum of Co 2p, two main peaks located at 781.1 (2p 3/2) and 796.8 eV (2p 1/2) are separated by about 15.7 eV (Fig. R3a, before catalytic reaction). For Co 2p 3/2, two distinguishable satellite peaks are located at about 786.4 eV (Sat.a) and 789.9 eV (Sat.b), and the intensity of Sat.a is much higher than that of Sat.b. It is generally accepted that the energy gap between the Co 2p main peaks and the satellite peaks can serve as an important standard, namely that the energy gap of Co(II) cation corresponds to ca. 6.0 eV, while the Co(III) cation typically features the energy gap to 9–10 eV.[S1] In this regard, the energy gap between Co 2p3/2 main peak and Sat.a is 5.3 eV (786.4 – 781.1), and the energy gap between Co 2p3/2 main peak and Sat.b is 8.8 eV (789.9 – 781.1), corresponding to the presence of Co(II) and Co(III) in the synthesized ZIF-67. After a rigorous calculation of the peak areas, there is 86% Co^{2+} and 14% Co^{3+} (Table R1). Similarly, after the catalytic reaction, the composition changed to 83% Co^{2+} and 17% Co^{3+}. Accordingly, the reaction mechanism is speculated to be related with the presence of Co^{3+} and Co^{2+} in ZIF-67.
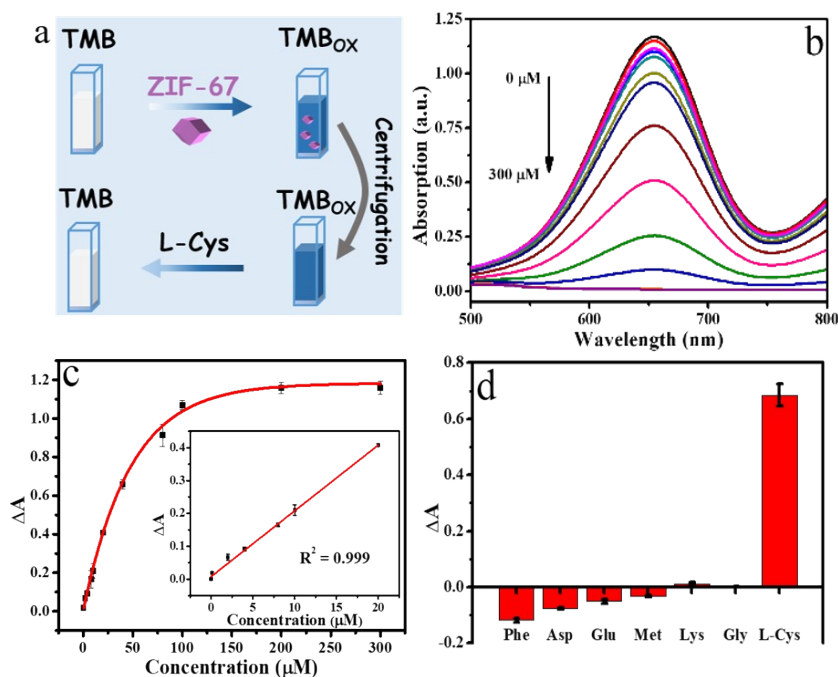
Fig. S10. (a) Schematic illustration of ZIF-67-TMB system for detection L-Cys. (b) UV-Vis spectra of system ZIF-67-TMB with ZIF-67 being centrifuged and separated vary with $C_{\text{L-Cys}}$. (c) Dose-response curve to detect L-Cys. The inset is a linear calibration plot. ΔA represents the difference of absorption intensity at 653 nm in the absence and presence of L-Cys. (d) Selectivity of the colorimetric assay towards L-Cys.

Table S3. Comparison of sensing performance for L-Cys with reported oxidase mimics

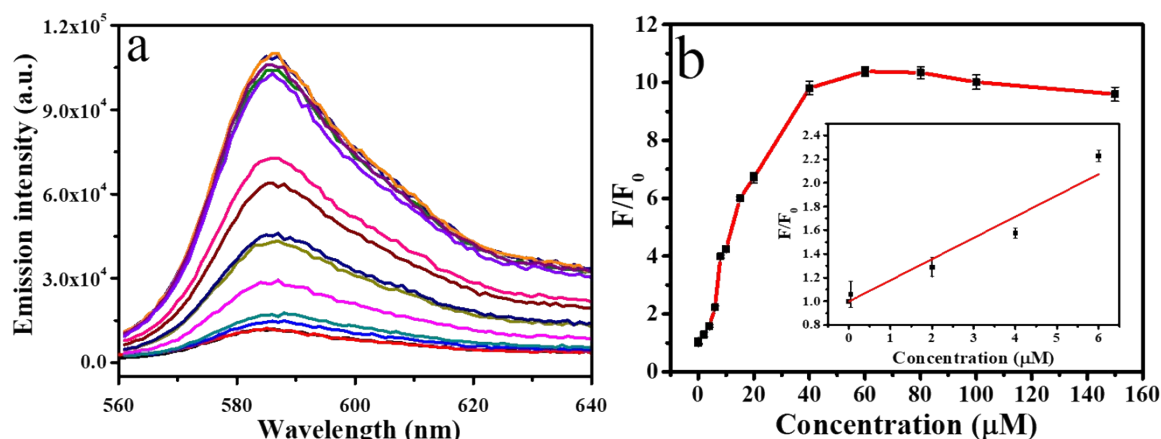| Oxidase Mimics	Detection Limit (nM)	Mode	Reference
Ce-MOF	135	turn-off	S12
$MnCo_2O_4$ NFs	34.3	turn-off	S13
perovskite $LaMnO_{3+\sigma}$ nanofibers	109.8	turn-off	S14
9-mesitylacridinium ion	100	turn-off	S15
ZIF-67	**31**	**turn-on**	**this work**

Fig. S11. (a) Emission intensity varies with concentrations of L-Cys in diluted human blood serum. (b) Dose-response curve to detect L-Cys. The inset is a linear calibration plot to detect L-Cys.

Table S4. Results of recovery studies of the analysis of L-Cys in diluted human blood

Add (µM)	Found (µM)	Recovery（%）
1	1.03±0.10	103
2.5	2.45±0.19	98
4	4.05±0.20	101

The practical application in diluted human serum is investigated as shown in Fig. S11. The fluorescence change was recorded with different $C_{\text{L-Cys}}$ (Fig. S11a). The dose-response curve about F/F_0 (fluorescence intensity in the presence (F) and absence (F_0) of L-Cys) versus $C_{\text{L-Cys}}$ is demonstrated (Fig. S11b), and a linear relationship between F/F_0 and $C_{\text{L-Cys}}$ ranging from 0.05 to 6 µM is presented inset of Fig. R8b. The fitting equation is $F/F_0 = 0.18C_{\text{L-Cys}} + 0.999$ ($R^2 = 0.97$). The measured detection limit is 94 nM (S/N = 3). Finally, a standard addition method was used to detect the level of L-Cys in diluted human blood serum as shown in Table S4. The recovery is 98%-103%.
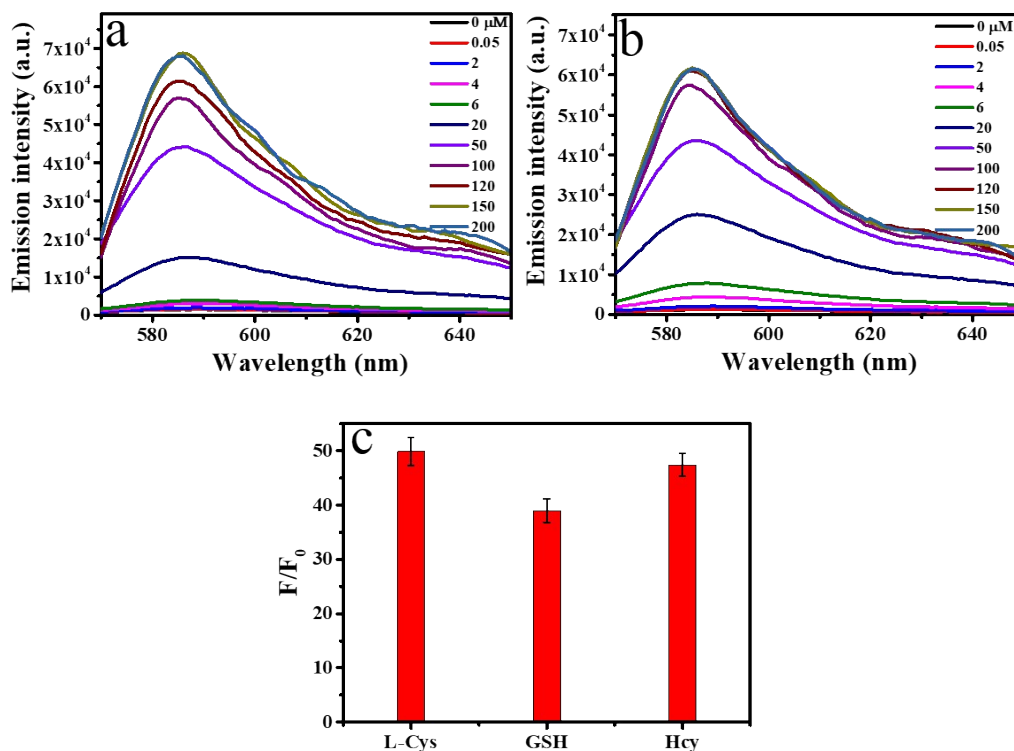
Fig. S12. Emission intensity varies with concentrations of GSH (a) and Hcy (b). (c) The reductive activity of 100 μM L-Cys, GSH and Hcy.

Hcy and GSH are also reductive biothiols. With oxAR$_2$ as a sensing probe, fluorescence responses to GSH (Fig. S12a) and Hcy (Fig. S12b) are recorded, respectively. Upon gradually increasing C_{GSH} or C_{Hcy} from 0 to 100 μM, the intensity of emission fluorescent at 585 nm enhances, exhibiting a "turn-on" sensing behavior. With 100 μM Hcy, GSH and L-Cys as examples, the reductive activity is evaluated as shown in Fig. S12c.

Additional References

S1   J. Qin, S. Wang and X. Wang, *Appl. Catal. B: Environmental*, 2017, **209**, 476-482.

S2   C.-J. Yu, T.-H. Chen, J.-Y. Jiang and W.-L. Tseng, *Nanoscale*, 2014, **6**, 9618-9624.

S3   X. Liu, Q. Wang, H. Zhao, L. Zhang, Y. Su and Y. Lv, *Analyst*, 2012, 137, 4552-4558.

S4   A. Asati, S. Santra, C. Kaittanis, S. Nath and J. M. Perez, *Angew. Chem. Int. Ed.*, 2009, **48**, 2308-2312.

S5   M. Huang, H. Wang, D. He, P. Jiang and Y. Zhang, *Chem. Commun.,* 2019, **55**, 3634-3637.

S6   Q. Wang, L. Zhang, C. Shang, Z. Zhang and S. Dong, *Chem. Commun.*, 2016, **52**, 5410-5413.

S7   N. Song, F. Ma, Y. Zhu, S. Chen, C. Wang and X. Lu, *ACS Sustainable Chem. Eng.*, 2018, **6**, 16766-16776.

S8   C. W. Lien, C. C. Huang and H. T. Chang, *Chem. Commun.*, 2012, **48**, 7952-7954.

S9   C. W. Tseng, H. Y. Chang, J. Y. Chang and C. C. Huang, *Nanoscale*, 2012, **4**, 6823-6830.

S10   C. W. Lien, B. Unnikrishnan, S. G. Harroun, C. M. Wang, J. Y. Chang, H. T. Chang and C. C. Huang, *Biosens. Bioelectron.*, 2018, **102**, 510-517.

S11   D. Li, B. Liu, P. J. Huang, Z. Zhang and J. Liu, *Chem. Commun.*, 2018, **54**, 12519-12522.

S12   Y. Xiong, S. Chen, F. Ye, L. Su, C. Zhang, S. Shen and S. Zhao, *Chem. Commun.*, 2015, **51**, 4635-4638.

S13   M. Gao, X. Lu, M. Chi, S. Chen and C. Wang, *Inorg. Chem. Front.*, 2017, **4**, 1862-1869.

S14   L. Song, Y. Zhu, Z. Yang, C. Wang and X. Lu, *J. Mater. Chem. B*, 2018, **6**, 5931-5939.

S15   J. Du, J. Wang, W. Huang, Y. Deng and Y. He, *Anal. Chem.*, 2018, **90**, 9959-9965.